Collision-Induced Dissociation and Theoretical Studies of Na^+−Acetonitrile Complexes

A. B. Valina, R. Amunugama, H. Huang, and M. T. Rodgers*

Department of Chemistry, Wayne State University, Detroit, Michigan 48202

Received: July 23, 2001; In Final Form: September 7, 2001

Collision-induced dissociation of $Na^+(CH_3CN)_x$, $x = 1-5$, with xenon is studied as a function of kinetic energy using guided ion beam mass spectrometry. In all cases, the primary and lowest energy dissociation channel observed is endothermic loss of one acetonitrile molecule. The cross section thresholds are interpreted to yield 0 and 298 K bond energies after accounting for the effects of multiple ion-molecule collisions, internal energy of the complexes, and dissociation lifetimes. Ab initio and density functional calculations at the MP2(full)/6-31G* and B3LYP/6-31G* levels of theory are used to determine the structures of these complexes and provide molecular constants necessary for the thermodynamic analysis of the experimental data. Theoretical bond dissociation energies are determined from single point calculations at the MP2(full)/6-311+G(2d,2p) and B3LYP/6-311+G(2d,2p) levels using the MP2(full)/6-31G* and B3LYP/6-31G* optimized geometries, respectively. The experimental bond energies determined here are in good agreement with previous experimental measurements for all complexes. Good agreement between theory and experiment is also found for all clusters except $x = 5$, where it is apparent that more basis functions are necessary to adequately describe the very weak noncovalent interactions in this complex.

Introduction

The complexation of metal ions to various ligands in solution can be strongly influenced by the solvent in which such interactions are examined. Gas-phase measurements of the binding interactions between metal ions and various ligands are free of solvent effects and allow the direct determination of absolute binding energies. Often, the trends observed in solution parallel those of the gas phase, but in some systems this is not the case. This is sometimes referred to as molecular recognition and is often the result of size effects or of competition between the ligand and the solvent for the metal ion. An interesting example of solvent-induced selectivity, reordering of the relative binding affinities, is observed for complexation of alkali metal ions to 18-crown-6. In the gas phase, the alkali metal ion binding affinity of 18-crown-6 follows the order $Na^+ > K^+ > Rb^+ > Cs^+$. This indicates that the charge density of the cation is the critical feature that controls the strength of binding.[1−3] This trend has been observed for a wide variety of ligands in the gas phase, and occurs because the smaller alkali metal ions have greater charge density, making it possible for them to get closer to the ligand to create a stronger electrostatic field to bind to the electron-donating atoms of the ligand. This behavior contrasts that found for 18-crown-6 in aqueous solution where the binding affinity follows the order $K^+ > Rb^+ > Cs^+ > Na^+$.[4] Insight into the aqueous selectivity of 18-crown-6 was gained by considering the competition between the solvation of the alkali cation and the complexation by crown ethers, reaction 1.[1−3] In

$$M^+(H_2O)_x + \text{18-crown-6} \rightarrow M^+(\text{18-crown-6}) + xH_2O \quad (1)$$

the theoretical study,[1] it was found that the aqueous selectivity could be mimicked with as few as four water molecules, whereas at least five water molecules were needed to mimic the aqueous selectivity using the experimentally determined binding energies.[2,3] This example suggests that accurate gas-phase measurements of binding energies between metal ions and various ligands combined with analogous measurements of solvation enthalpies can be used to provide a better understanding of such interactions in solution. A particularly important aspect of such gas-phase studies is that the measurement of solvation enthalpies of metal ions can be potentially useful in the study of a wide variety of ligands. This provides motivation for the work performed here as well as a series of related studies currently being performed in our laboratory in which the solvation enthalpies of a variety of metal ions are being examined to commonly used solvents. An extensive number of studies of the solvation enthalpies of metal ions to water have been conducted.[5−26] Studies of the solvation enthalpies of metal ions to other commonly used solvents such as CH_3OH,[19,25−34] C_2H_5OH,[19,25,26,31−33] CH_3CN,[19,25,26,35−37] $(CH_3)_2CO$,[19,24−27,34,38,39] and $(CH_3)_2SO$[19,25,26,35] have been much more limited in scope. In many of the studies performed thus far, measurements have been limited to determination of the enthalpy of solvation for the first or the first and second solvent molecule. As the 18-crown-6 example indicates, it is probably necessary to include more than one or two solvent molecules. Thus, it is desirable to have accurate quantitative measurements of the enthalpies of solvation for at least four solvent molecules. However, some systems may not mimic solution behavior until higher degrees of solvation are achieved and thus accurate quantitative measurements beyond four solvent molecules is also desirable.

In recent work, we have developed methods to allow the application of quantitative threshold collision-induced dissociation (CID) methods to obtain accurate thermodynamic information on increasingly large systems.[16,31−33,39−48] One of the driving forces behind these developments is our interest in applying such techniques to large systems such as those of biological relevance. In addition, we seek to perform accurate thermochemical measurements that provide absolute anchors for metal cation affinity scales over an ever-broadening range of energies and molecular systems. In the present study, we use guided ion beam mass spectrometry to collisionally excite

10.1021/jp0128123 CCC: $20.00
Published on Web 11/17/2001

$Na^+(CH_3CN)_x$ clusters. The kinetic energy-dependent cross sections for the CID processes are analyzed using methods developed previously.[40] The analysis explicitly includes the effects of the internal and translational energy distributions of the reactants, multiple collisions, and the lifetime for dissociation. We derive $(CH_3CN)_{x-1}Na^+-CH_3CN$, $x = 1-5$ bond dissociation energies (BDEs) for all of the complexes and compare these results to ab initio and density functional calculations performed here. Comparison is also made to previous experimental studies.[35]

Previous work aimed at determination of the thermodynamics of $M^+(CH_3CN)_x$ clusters has been carried out by several groups using a variety of techniques. Equilibrium measurements in a Fourier transform ion cyclotron resonance mass spectrometer (FT-ICR) were carried out to determine the binding energy of Li^+ to CH_3CN[25] and of Na^+ to CH_3CN.[26] Equilibrium measurements in a high-pressure mass spectrometer (HPMS) have also been performed to determine the binding energies of $M^+(CH_3CN)_x$, $x = 2-5$ for Na^+, and $x = 1-5$ for K^+, Rb^+, and Cs^+,[35] to $Ag^+(CH_3CN)_x$, $x = 1$ and 2,[19] and to $Cu^+(CH_3CN)_x$, $x = 1$ and 2.[36] The binding energies of $Ag^+(CH_3CN)_x$, $x = 1$ and 2, were also recently remeasured by threshold CID in a triple quadrupole instrument.[37] In addition, ligand switching reactions carried out in a selected ion flow tube were used to measure rate constants for a variety of ligands binding to Na^+ including CH_3CN.[49] Although rates were measured for clusters containing up to three CH_3CN ligands in this work, a binding energy was deduced only for the cluster with one CH_3CN ligand.

Experimental Section

General Procedures. Cross sections for collision-induced dissociation of $Na^+(CH_3CN)_x$ clusters are measured using a guided ion beam mass spectrometer that has been described in detail previously.[45] The $Na^+(CH_3CN)_x$ clusters are generated as described below. The ions are extracted from the source, accelerated, and focused into a magnetic sector momentum analyzer for mass analysis. Mass-selected ions are decelerated to a desired kinetic energy and focused into an octopole ion guide, which traps the ions in the radial direction.[50] The octopole passes through a static gas cell containing xenon, used as the collision gas, for reasons described elsewhere.[51-53] Low gas pressures in the cell (typically 0.05−0.20 mTorr) are used to ensure that multiple ion-molecule collisions are improbable. Product and unreacted beam ions drift to the end of the octopole where they are focused into a quadrupole mass filter for mass analysis and subsequently detected with a secondary electron scintillation detector and standard pulse counting techniques.

Ion intensities are converted to absolute cross sections, as described previously.[54] Absolute uncertainties in cross section magnitudes are estimated to be ±20%, which are largely the result of errors in the pressure measurement and the length of the interaction region. Relative uncertainties are approximately ±5%.

Ion kinetic energies in the laboratory frame, E_{lab}, are converted to energies in the center of mass frame, E_{CM}, using the formula $E_{CM} = E_{lab}\, m/(m + M)$, where M and m are the masses of the ionic and neutral reactants, respectively. All energies reported below are in the CM frame unless otherwise noted. The absolute zero and distribution of the ion kinetic energies are determined using the octopole ion guide as a retarding potential analyzer, as previously described.[54] The distribution of ion kinetic energies is nearly Gaussian with a fwhm typically between 0.2 and 0.4 eV (lab) for these experiments. The uncertainty in the absolute energy scale is ±0.05 eV (lab).

Even when the pressure of the reactant neutral is low, it has previously been demonstrated that the effects of multiple collisions can significantly influence the shape of CID cross sections.[55] Because the presence and magnitude of these pressure effects is difficult to predict, we have performed pressure-dependent studies of all cross sections examined here. In the present systems, we observe small cross sections at low energies that have an obvious dependence upon pressure. We attribute this to multiple energizing collisions that lead to an enhanced probability of dissociation below threshold as a result of the longer residence time of these slower moving ions. Data free from pressure effects are obtained by extrapolating to zero reactant pressure, as described previously.[55] Thus, results reported below are due to single bimolecular encounters.

Ion Source. The $Na^+(CH_3CN)_x$ clusters are formed in a 1−1.5 m long flow tube[45] operating at a pressure of 0.7−1.1 Torr with a helium flow rate of 4000−7000 sccm. Sodium ions are generated in a continuous dc discharge by argon ion sputtering of a cathode, made from tantalum, with a cavity containing sodium metal. Typical operating conditions of the discharge for sodium ion production are 1.5−2.5 kV and 15−25 mA in a flow of roughly 10% argon in helium. The $Na^+(CH_3CN)_x$ clusters are formed by associative reactions of the sodium ion with acetonitrile molecules that are introduced into the flow 20−50 cm downstream from the dc discharge. The flow conditions used in this ion source provide in excess of 10^5 collisions between an ion and the buffer gas, which should thermalize the ions both vibrationally and rotationally. In our analysis of the data, we assume that the ions produced in this source are in their ground electronic states and that the internal energy of the $Na^+(CH_3CN)_x$ clusters is well described by a Maxwell-Boltzmann distribution of ro-vibrational states at 300 K. Previous work from this[42,44-47] and the Armentrout laboratories has shown that these assumptions are generally valid.[51,55-59]

Thermochemical Analysis. The threshold regions of the reaction cross sections are modeled using eq 2, where σ_0 is an energy independent scaling factor, E is the relative translational

$$\sigma(E) = \sigma_0 \sum_i g_i (E + E_i - E_0)^n / E \qquad (2)$$

energy of the reactants, E_0 is the threshold for reaction of the ground electronic and ro-vibrational state, and n is an adjustable parameter. The summation is over the ro-vibrational states of the reactant ions, i, where E_i is the excitation energy of each state and g_i is the population of those states ($\sum g_i = 1$). The populations of excited ro-vibrational levels are not negligible even at 298 K as a result of the many low-frequency modes present in these ions. The relative reactivity of all ro-vibrational states, as reflected by σ_0 and n, is assumed to be equivalent.

The Beyer-Swinehart algorithm[60] is used to evaluate the density of the ro-vibrational states, and the relative populations, g_i, are calculated by an appropriate Maxwell-Boltzmann distribution at the 298 K temperature appropriate for the reactants. The average vibrational energy at 298 K of the $Na^+(CH_3CN)_x$ clusters are also given in Table S1. We have estimated the sensitivity of our analysis to the deviations from the true frequencies by scaling the calculated frequencies to encompass the range of average scaling factors needed to bring calculated frequencies into agreement with experimentally determined frequencies found by Pople et al.[61] Thus, the originally calculated vibrational frequencies were increased and decreased by 10%. The corresponding change in the average vibrational

energy is taken to be an estimate of one standard deviation of the uncertainty in vibrational energy (Table S1) and is included in the uncertainties, also reported as one standard deviation, listed with the E_0 values.

We also consider the possibility that collisionally activated complex ions do not dissociate on the time scale of our experiment (about 10^{-4} s, but energy dependent) by including statistical theories for unimolecular dissociation, specifically Rice-Ramsperger-Kassel-Marcus (RRKM) theory, into eq 2 as described in detail elsewhere.[40,58] This requires sets of rovibrational frequencies appropriate for the energized molecules and the transition states (TSs) leading to dissociation. The former sets are given in Tables S1 and S2, whereas we assume that the TSs are loose and product-like because the interaction between the sodium ion and the acetonitrile molecules is largely electrostatic. In this case, the TS vibrations used are the frequencies corresponding to the products, which are also found in Table S1. The transitional frequencies, those that become rotations and translations of the completely dissociated products, are treated as rotors, a treatment that corresponds to a phase space limit (PSL) and is described in detail elsewhere.[40] Briefly, two of the rotors are simply the two rotational constants of the CH_3CN product with axes that are perpendicular to the reaction coordinate and correspond to the 2D rotational constant (0.30 cm^{-1}). In the $Na^+(CH_3CN)$ system, which yields one atomic product, these are the only two transitional modes. For the larger clusters, three additional transitional modes exist. Two of these rotors are the rotational constants of the $Na^+(CH_3CN)_{x-1}$ product, again those that are perpendicular to the reaction coordinate. Of the two rotational constants of the products with axes lying along the reaction coordinate, one is a transitional mode and is assigned as the remaining rotational constant of the CH_3CN product (5.31 cm^{-1}). The other becomes the 1-D external rotor of the TS. These are listed in Table S2. The external rotations of the energized molecule and TS are also included in the modeling of the CID data. The external rotational constants of the TS are determined by assuming that the TS occurs at the centrifugal barrier for interaction of $Na^+(CH_3CN)_{x-1}$ with the neutral CH_3CN molecule, calculated variationally as outlined elsewhere.[40] The 2-D external rotations are treated adiabatically but with centrifugal effects included, consistent with the discussion of Waage and Rabinovitch.[62] In the present work, the adiabatic 2-D rotational energy is treated using a statistical distribution with explicit summation over the possible values of the rotational quantum number, as described in detail elsewhere.[3]

The model represented by eq 2 is expected to be appropriate for translationally driven reactions[63] and has been found to reproduce reaction cross sections well in a number of previous studies of both atom-diatom and polyatomic reactions,[64,65] including CID processes.[51,55,57,58,66−68] The model is convoluted with the kinetic energy distributions of both the reactant cluster ion and neutral xenon atom, and a nonlinear least-squares analysis of the data is performed to give optimized values for the parameters σ_0, E_0, and n. The error associated with the measurement of E_0 is estimated from the range of threshold values determined for different zero-pressure extrapolated data sets, variations associated with uncertainties in the vibrational frequencies, and the error in the absolute energy scale, 0.05 eV (lab). For analyses that include the RRKM lifetime effect, the uncertainties in the reported E_0 values also include the effects of increasing and decreasing the time assumed available for dissociation (or equivalently, the distance traveled between the collision and detection) by a factor of 2.

Equation 2 explicitly includes the internal energy of the ion, E_i. All energy available is treated statistically, which should be a reasonable assumption because the internal (rotational and vibrational) energy of the reactants is redistributed throughout the ion upon impact with the collision gas. The threshold for dissociation is by definition the minimum energy required, leading to dissociation, and thus corresponds to formation of products with no internal excitation. The assumption that products formed at threshold have an internal temperature of 0 K has been tested for several systems.[31−33,51,52,57,58] It has also been shown that treating all energy of the ion (vibrational, rotational, and translational) as capable of coupling into the dissociation coordinate leads to reasonable thermochemistry. The threshold energies for dissociation reactions determined by analysis with eq 2 are converted to 0 K bond energies by assuming that E_0 represents the energy difference between reactants and products at 0 K.[69] This assumption requires that there are no activation barriers in excess of the endothermicity of dissociation. This is generally true for ion-molecule reactions[64] and should be valid for the simple heterolytic bond fission reactions examined here.[70]

Theoretical Calculations. To obtain model structures, vibrational frequencies, and energetics for the neutral CH_3CN molecule and the $Na^+(CH_3CN)_x$ clusters, ab initio and density functional calculations were performed using Gaussian 98.[71] Geometry optimizations were performed at the MP2(full)/6-31G* and B3LYP/6-31G* levels.[72−74] Vibrational analyses of the geometry optimized structures were performed to determine the vibrational frequencies of the reactant and product cluster ions, $Na^+(CH_3CN)_x$ and neutral CH_3CN molecule. When used to model the data or to calculate thermal energy corrections, the MP2(full)/6-31G* vibrational frequencies are scaled by a factor of 0.9646 and the B3LYP/6-31G* vibrational frequencies are scaled by a factor of 0.9804.[75] The scaled vibrational frequencies thus obtained for the systems studied are available as Supporting Information and listed in Table S1, while Table S2 lists the rotational constants. Single point energy calculations were performed at the MP2(full)/6-311+G(2d,2p) and B3LYP/6-311+G(2d,2p) levels using the MP2(full)/6-31G* and B3LYP/6-31G* optimized geometries, respectively. To obtain accurate bond dissociation energies, zero point energy (ZPE) corrections were applied and basis set superposition errors (BSSE) were subtracted from the computed dissociation energies in the full counterpoise approximation.[76,77] The ZPE corrections are small, vary with the size of the cluster, and are 2.8, 3.0, and 1.9 kJ/mol for the MP2 values for the $Na^+(CH_3CN)_x$ clusters, $x = 1-3$, and 2.8, 2.9, 2.2, 2.0, and 1.4 kJ/mol for the B3LYP values for the $Na^+(CH_3CN)_x$ clusters, $x = 1-5$, respectively. Similarly, the BSSE corrections are small, and range from 1.5 to 2.9 kJ/mol for the B3LYP values. The BSSE corrections are somewhat larger for the MP2 calculations and range from 5.6 to 8.4 kJ/mol.

Results

Cross Sections for Collision-Induced Dissociation. Experimental cross sections are shown in Figure 1 for the interaction of $Na^+(CH_3CN)_x$, $x = 1-5$, clusters with xenon. The sequential loss of intact acetonitrile molecules and ligand exchange with xenon are the only processes observed in these systems over the collision energy range studied, typically 0 to >7.5 eV. The primary (most favorable) process for all clusters is the loss of a single acetonitrile molecule in the CID reactions 3. As the

$$Na^+(CH_3CN)_x + Xe \rightarrow Na^+(CH_3CN)_{x-1} + CH_3CN + Xe \quad (3)$$

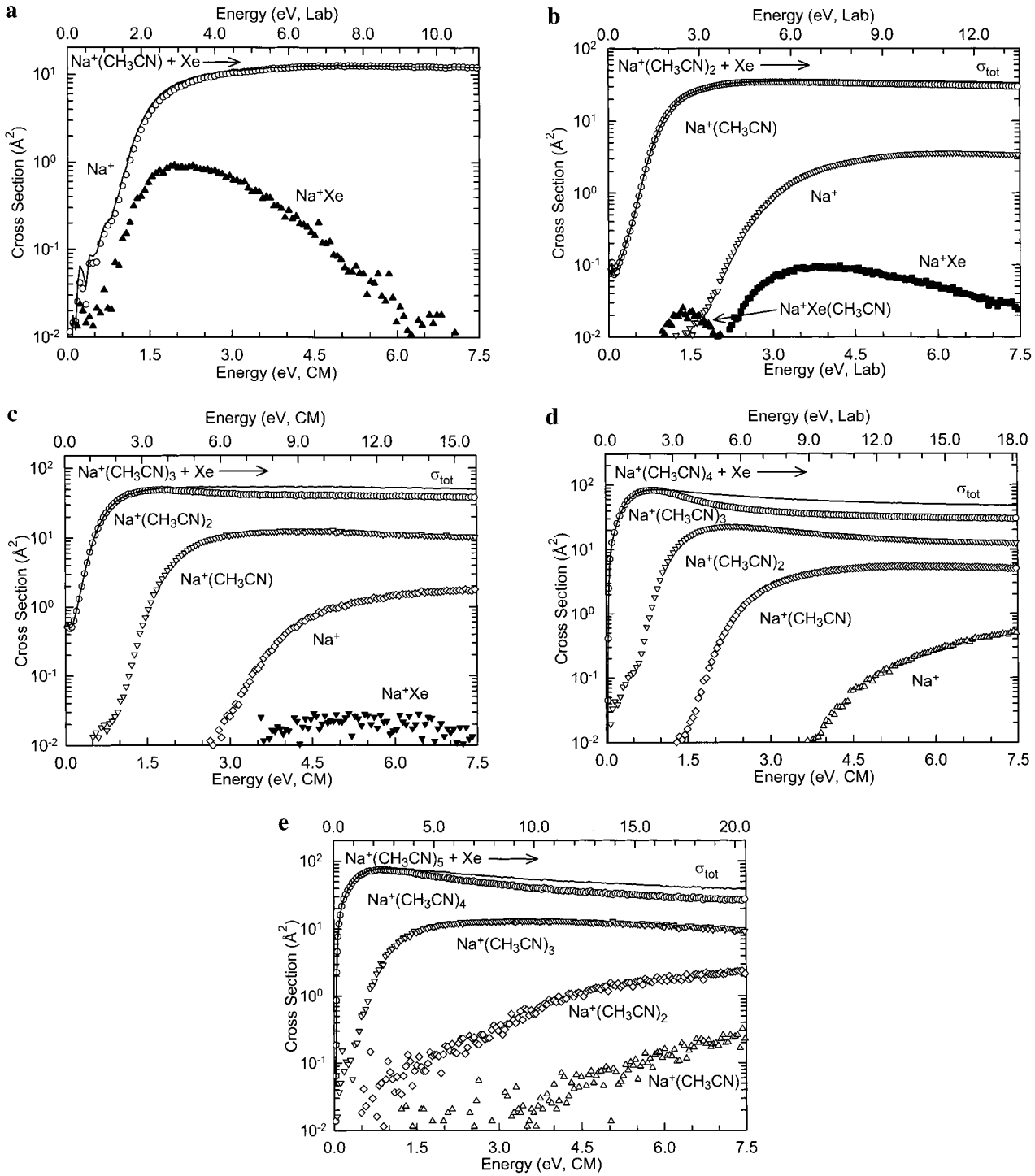

Figure 1. Cross sections for the collision-induced dissociation of $Na^+(CH_3CN)_x$, $x = 1-5$ (parts a through e, respectively), with Xe as a function of the kinetic energy in the center-of-mass frame (lower *x*-axis) and laboratory frame (upper *x*-axis). Data are shown for a Xe pressure of ~0.2 mTorr. Primary, secondary, tertiary, and quaternary product cross sections are shown as ○, ▽, ◇, and △, respectively. Primary, secondary, and tertiary ligand exchange product cross sections are shown as ▲, ■, and ▼, respectively.

size of the cluster increases, the maximum cross section for reaction 2 (as well as the total cross section) increases in magnitude in a manner roughly consistent with the percentage increase in ligands. As the size of the cluster increases, the threshold for reaction 3 decreases, consistent with conventional ideas of ligation of gas-phase ions; i.e., stepwise sequential bond energies decrease because of increasing electrostatic repulsion between the ligands, causing the distance between the cation and ligands to increase. Such ideas have been noted in previous experimental and theoretical studies of $M^+(ligand)_x$ clusters.[6,14,35,78]

Dissociation of additional CH_3CN ligands is observed for the larger clusters. For $x = 2$, loss of a second CH_3CN molecule is observed at higher energies. For $x = 3$, loss of a third CH_3CN molecule is observed at even higher energies. For $x = 4$, loss of a fourth CH_3CN molecule is observed at even higher energies. For $x = 5$, loss of a fifth CH_3CN molecule is not observed over the energy range examined here. As the size of the cluster

increases, secondary, tertiary, and quaternary dissociation account for increasingly greater percentages of the total cross section, approximately 10, 24, 38, and 32% for $x = 2-5$, respectively, at the highest energies examined.

The cross sections for ligand exchange decrease as the size of the cluster increases. For the case of $x = 1$, the cross section for the ligand exchange process is substantial, having a maximum nearly 10% as large as the CID process. For the $x = 2$ cluster, the ligand exchange cross section has dropped by more than an order of magnitude. For larger clusters, the efficiencies of the ligand exchange processes drop off rapidly enough that they could not be measured for clusters with greater than three acetonitrile molecules.

$Na^+(CH_3CN)$ + Xe. Results for the interaction of $Na^+(CH_3CN)$ with xenon are shown in Figure 1a. The major product is Na^+, which has an apparent threshold of 0.5 eV and a maximum cross section of ∼11 Å^2. The ligand exchange product Na^+Xe is observed with an apparent threshold of 0.4 eV and a maximum cross section of almost 1 Å^2 at 2.0 eV, which drops off rapidly with energy due to competition with the primary CID process. Because the Na^+Xe ligand exchange product cross section has a lower threshold than the Na^+ product and a modest magnitude, it seems plausible that the apparent threshold for the CID process may be shifted to energies higher than the true thermodynamic threshold by competition with this ligand exchange process, a competitive shift. We do not believe this is a problem in this system as the threshold measured here for the CID process is in good agreement with the theoretical values calculated, as will be discussed below.

$Na^+(CH_3CN)_2$ + Xe. Results for the interaction of $Na^+(CH_3CN)_2$ with xenon are shown in Figure 1b. The major product is $Na^+(CH_3CN)$. The loss of one acetonitrile molecule from this species begins at an apparent threshold near 0 eV with a cross section that is more than twice as large as that of the monoligated ion. The secondary product of this reaction, Na^+, has an apparent threshold of ∼1.5 eV. Two ligand exchange products are observed, $Na^+(CH_3CN)Xe$ and Na^+Xe. The primary ligand exchange product, $Na^+(CH_3CN)Xe$, rises from an apparent threshold near 1 eV to a maximum of 0.3 Å^2 at approximately 1.4 eV. At higher energies, it falls off rapidly due to competition with the primary CID process. The secondary ligand exchange product, Na^+Xe, slowly grows in from an apparent threshold near 2.2 eV to a maximum of 0.1 Å^2 at approximately 3.8 eV. At higher energies, it falls off due to competition with the secondary CID process.

$Na^+(CH_3CN)_3$ + Xe. Results for the interaction of $Na^+(CH_3CN)_3$ with xenon are shown in Figure 1c. The CID behavior for the triply ligated Na^+ is notably different from the doubly ligated ion. The major product is $Na^+(CH_3CN)_2$. The loss of one acetonitrile molecule from the reactant cluster begins at an apparent threshold near 0 eV with a cross section that is roughly 50% larger at its maximum than the maximum observed for the loss of one acetonitrile molecule from the doubly ligated ion. The cross section for production of the primary product decreases as the secondary $Na^+(CH_3CN)$ product appears. The threshold for the secondary product appears at ∼0.7 eV with a maximum cross section of ∼13 Å^2 and then drops off slowly as the tertiary product, Na^+, grows in from an apparent threshold near 2.8 eV. The Na^+ product reaches a maximum cross section of ∼1.8 Å^2 at the highest energies examined. Only one ligand exchange product is observed. The primary ligand exchange product, $Na^+(CH_3CN)_2Xe$, and secondary ligand exchange product, $Na^+(CH_3CN)Xe$, are not observed. The tertiary ligand exchange product, Na^+Xe, rises from an apparent threshold near 3.5 eV to a maximum cross section of 0.03 Å^2 at approximately 5.5 eV.

$Na^+(CH_3CN)_4$ + Xe. Results for the interaction of $Na^+(CH_3CN)_4$ with xenon are shown in Figure 1d. The CID behavior for the quadruply ligated Na^+ is similar to that observed for the triply ligated system, except that at higher energies the secondary, tertiary, and quaternary dissociation processes account for a greater percentage of the total cross section. The apparent threshold for the primary product, $Na^+(CH_3CN)_3$ appears near 0 eV with a cross section that is ∼50% greater than the triply ligated species at their respective maxima. The cross section for production of the primary product decreases slightly more rapidly than for the triply ligated species, beginning at the apparent threshold for the secondary $Na^+(CH_3CN)_2$ product. The $Na^+(CH_3CN)_2$ product has an apparent threshold of ∼0.4 eV and a maximum cross section of ∼30 Å^2, which drops off slowly as the tertiary product, $Na^+(CH_3CN)$, grows in. The apparent threshold for the $Na^+(CH_3CN)$ product occurs near 1.4 eV and reaches a maximum cross section of ∼8 Å^2, which declines very slowly as the quaternary product, Na^+ grows in. The apparent threshold for the Na^+ product occurs near 3.7 eV and reaches a maximum cross section of ∼0.8 Å^2 at the highest energies examined. The ligand exchange product channels were monitored; however, signals were sufficiently small that they were not discernible from noise.

$Na^+(CH_3CN)_5$ + Xe. Results for the interaction of $Na^+(CH_3CN)_5$ with xenon are shown in Figure 1e. The CID behavior for the quintuply ligated Na^+ is similar to that observed for the cluster containing one less acetonitrile molecule. The apparent threshold for the primary product, $Na^+(CH_3CN)_4$, appears near 0 eV with a cross section that is ∼10% smaller than the quadruply ligated species at their respective maxima. The cross section for production of the primary product decreases rapidly at the apparent threshold for the secondary $Na^+(CH_3CN)_3$ product. The $Na^+(CH_3CN)_3$ product has an apparent threshold of ∼0.1 eV and a maximum cross section of ∼13 Å^2, which drops off slowly as the tertiary product, $Na^+(CH_3CN)_2$, grows in. The apparent threshold for the $Na^+(CH_3CN)_2$ product occurs near 0.8 eV and reaches a maximum cross section of ∼3 Å^2 at the highest energies examined. Although the $Na^+(CH_3CN)_2$ product does not decline as the quaternary product, $Na^+(CH_3CN)$, grows in, the rise in the cross section changes slope at the apparent threshold for this product. The apparent threshold for the $Na^+(CH_3CN)$ product occurs near 3.7 eV and reaches a maximum cross section of ∼0.3 Å^2 at the highest energies examined. The Na^+ product, which is not expected to be formed very efficiently, is not observed over the range of energies examined. The ligand exchange product channels were again too small to distinguish from noise.

Threshold Analysis. The model of eq 2 was used to analyze the thresholds for reactions 3 in all five $Na^+(CH_3CN)_x$ systems. As previously discussed,[51,57,58] we believe the analysis of the primary CID thresholds provides the most reliable thermochemistry for such studies. This is because secondary and higher order products are more sensitive to lifetime effects, and additional assumptions are needed to quantitatively include the multiple products formed. The results of these analyses are provided in Table 1. Two values of E_0 are listed: one without the RRKM lifetime analysis and one where the lifetime analysis is included (a loose PSL TS model). Comparison of the two E_0 values shows that the kinetic shifts observed for these systems increase with

TABLE 1: Fitting Parameters of Eq 2, Threshold Dissociation Energies at 0 K, Kinetic Shifts, and Entropies of Activation at 1000 K of $Na^+(CH_3CN)_x$, $x = 1-5$[a]

species	σ_0[b]	n[b]	E_0[c] (eV)	E_0(PSL) (eV)	kinetic shift (eV)	$\Delta S^{\ddagger}$(PSL) (J mol^{-1} K^{-1})
$Na^+(CH_3CN)$	15.5 (0.9)	1.1 (0.1)	1.32 (0.05)	1.32 (0.05)	0.00	17 (2)
$Na^+(CH_3CN)_2$	60.0 (7.3)	0.9 (0.1)	1.21 (0.10)	1.13 (0.08)	0.08	−2 (5)
$Na^+(CH_3CN)_3$	105.7 (2.4)[d]	0.7 (0.1)[d]	1.07 (0.04)[d]	0.92 (0.03)[d]	0.15[d]	32 (3)[d]
	104.2 (3.0)[e]	0.8 (0.1)[e]	1.07 (0.04)[e]	0.93 (0.03)[e]	0.14[e]	32 (3)[e]
$Na^+(CH_3CN)_4$	112.4 (1.3)[d]	0.7 (0.1)[d]	0.89 (0.04)[d]	0.67 (0.03)[d]	0.22[d]	14 (4)[d]
	114.9 (2.5)[e]	0.8 (0.1)[e]	0.91 (0.04)[e]	0.66 (0.03)[e]	0.25[e]	14 (4)[e]
$Na^+(CH_3CN)_5$	98.8 (2.1)[d]	1.0 (0.1)[d]	0.99 (0.02)[d]	0.55 (0.04)[d]	0.44[d]	39 (4)[d]
	98.2 (2.3)[e]	1.0 (0.1)[e]	1.02 (0.03)[e]	0.54 (0.03)[e]	0.48[e]	39 (4)[e]

[a] Uncertainties are listed in parentheses. [b] Average values for loose PSL transition state. [c] No RRKM analysis. [d] Average values obtained when fitting the total cross section. [e] Average values obtained when fitting the channel corresponding to the loss of one acetonitrile molecule.

the number of acetonitrile molecules surrounding the sodium ion. Thus dissociation of the $Na^+(CH_3CN)$ system shows no kinetic shift, while $Na^+(CH_3CN)_5$ exhibits a kinetic shift of 0.46 ± 0.02 eV. The total number of vibrations increases with the size of the cluster from 15 for $Na^+(CH_3CN)$ to 87 for $Na^+(CH_3CN)_5$. Likewise, the number of heavy atoms increases from 4 to 16 as the size of the cluster increases from one to five CH_3CN molecules. Thus the number of low frequency vibrations, those resulting in the largest impact on the density of states and therefore lifetime of the dissociating cluster, increase with the size of the cluster. This implies that the observed kinetic shift should directly correlate with the size of the cluster ion, which is exactly what is observed (Table 1).

Experimental cross sections and fits to the data using a loose PSL model are shown in Figure 2 for loss of a single acetonitrile molecule in the interaction of $Na^+(CH_3CN)_x$, $x = 1-5$, clusters with Xe (reaction 3). In all cases, the experimental cross sections for reactions 3 are accurately reproduced using a loose PSL TS model.[40] Previous work has shown that this model provides the most accurate assessment of the kinetic shifts for CID processes for electrostatic ion-molecule complexes.[31−33,39−43,45,66,67] This conclusion will be tested further here by comparison of these values with the results of Davidson and Kebarle (DK)[35] below. Good reproduction of the data is obtained over energy ranges exceeding 1.0 eV and cross section magnitudes of at least a factor of 100. For the $x = 3-5$ clusters, the cross sections are still finite at the lowest energies we examine, and hence the reproduction does not cover quite the same magnitude range.

Two sets of fitting parameters are listed in Table 1 for the $Na^+(CH_3CN)_x$, $x = 3-5$, clusters. These represent analysis of the total cross section for dissociation and an analysis of the cross section for loss of a single acetonitrile molecule. Experimental cross sections and fits to the total CID cross section using a loose PSL TS model are shown in Figure 3 for the interaction of $Na^+(CH_3CN)_x$, $x = 3-5$, clusters with Xe. For the $x = 1$ and 2 clusters, these two models give identical results. For the larger clusters, $x = 3-5$, the fitting parameters obtained using the two models differ slightly, but result in threshold values that differ by only 0.01 eV. In these systems, the cross sections for reactions 3 are strongly affected by subsequent dissociation shortly after the threshold, such that the energy range unaffected by this second-order process is narrow. As a result, the fits of the total cross section could be carried out over a more extensive energy range than those for the primary dissociation channel.

The entropy of activation, $\Delta S^{\ddagger}$, is a measure of the looseness of the TS and also a reflection of the complexity of the system. It is largely determined by the molecular parameters used to model the energized molecule and the TS, but it also depends on the threshold energy. Listed in Table 1, $\Delta S^{\ddagger}$(PSL) values at 1000 K show modest variation, as expected on the basis of the similarity of these systems, and range between −2 and +39 J K^{-1} mol^{-1} across these systems. These entropies of activation can be favorably compared to a wide variety of noncovalently bound complexes previously measured in our laboratory, and to the $\Delta S^{\ddagger}_{1000}$ values in the range 29−46 J K^{-1} mol^{-1} collected by Lifshitz for several simple bond cleavage dissociations of ions.[79]

Theoretical Results. Theoretical structures for neutral CH_3CN ligand and for the clusters of $Na^+(CH_3CN)_x$, $x = 1-5$, were calculated as described above. Table 2 gives details of the final geometries for each of these species at both the MP2-(full)/6-31G* and B3LYP/6-31G* levels of theory. The MP2 and B3LYP optimized geometries are very similar. Results for the most stable B3LYP conformation of each $Na^+(CH_3CN)_x$ cluster are shown in Figure 4.[80]

As pointed out earlier,[35] aprotic solvents are characterized by a permanent dipole in which the positive charge is diffusely distributed over a large part of the molecule while the negative charge is concentrated in a small, accessible end of the molecule. This corresponds to the lone pair of electrons on the cyano nitrogen atom. Thus it is not surprising that the calculations find that the Na^+ ion prefers to be bound to the lone pair of electrons on the cyano nitrogen atom along the axis of the molecule, rather than to the π-electrons of the C≡N bond. The distortion of the CH_3CN molecule that occurs upon complexation to the Na^+ ion is very minor. The change in geometry is largest for the smallest cluster, $Na^+(CH_3CN)$, and decreases with increasing number of solvent molecules. Bond lengths and bond angles change in the most extreme cases by less than 0.004 Å and 0.5°, respectively. The arrangement of the CH_3CN molecules around the sodium ion in the $Na^+(CH_3CN)_x$ clusters is very nearly the ideal structures predicted by the valence shell electron pair repulsion (VSEPR) model, e.g., linear for $x = 1$ and 2, trigonal planar for $x = 3$, tetrahedral for $x = 4$, and trigonal bipyramidal for $x = 5$.

As mentioned above, the MP2 and B3LYP optimized geometries are very similar. The B3LYP structures have slightly shorter Na^+-N bond lengths, although the differences diminish with increasing cluster size. The shorter Na^+-N bond lengths are consistent with the larger BDEs calculated at the B3LYP level of theory. The difference in the calculated MP2 and B3LYP BDEs also diminishes with increasing cluster size, again consistent with the smaller differences in the Na^+-N bond lengths as the size of the cluster increases. The C≡N and C−C bond lengths are also very slightly shorter, and the C−H bond lengths are just slightly longer in the B3LYP structures and show little or no variation with the size of the cluster. Almost no differences are observed in the MP2 and B3LYP ∠NNa^+N, ∠Na^+NC, and ∠NCC bond angles. Whereas, the ∠CCH and ∠HCH bond angles in the B3LYP structures are consistently 0.2° larger and 0.2° smaller for all clusters, respectively.

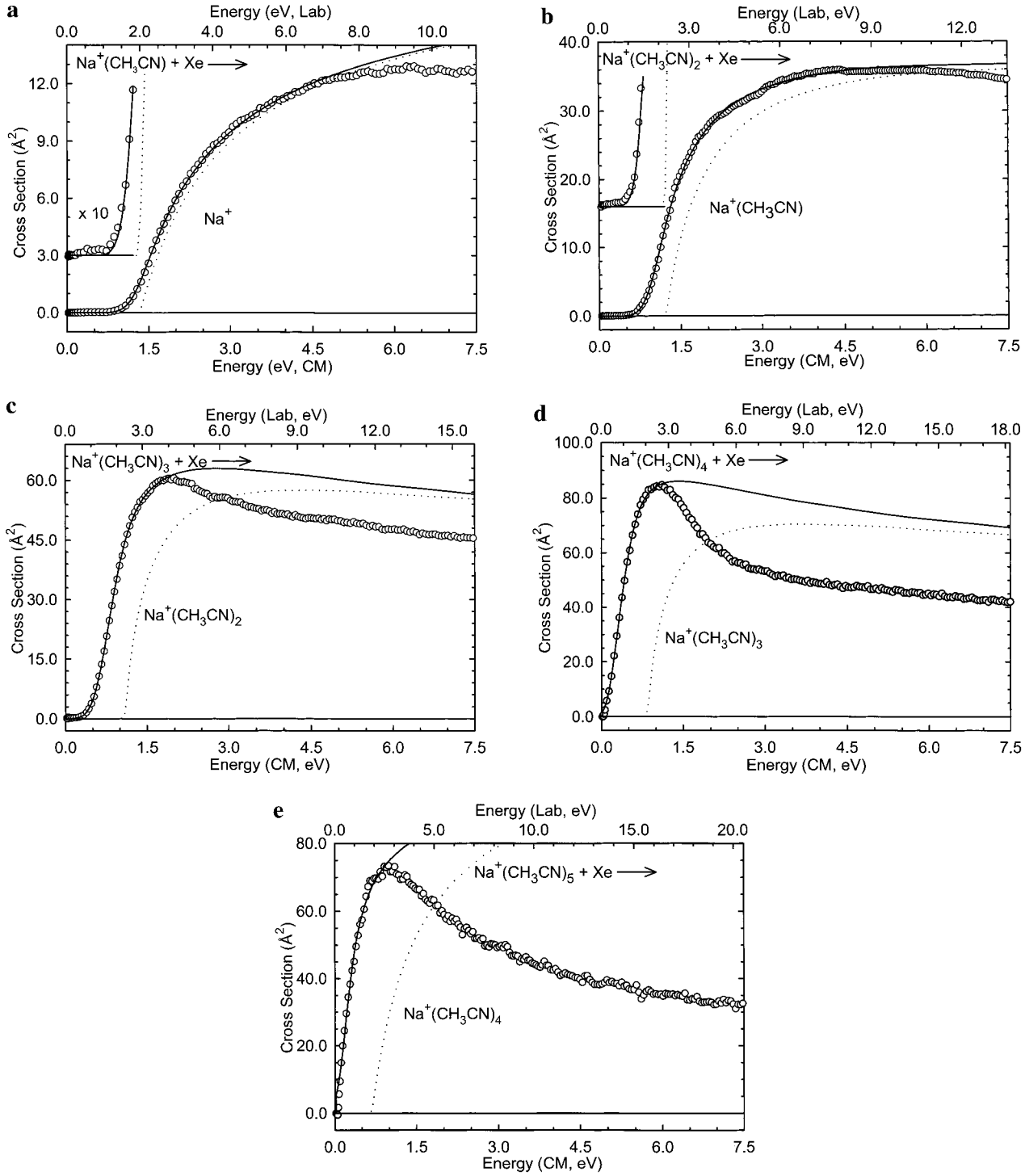

Figure 2. Zero-pressure-extrapolated primary product cross section for collision-induced dissociation of the $Na^+(CH_3CN)_x$, $x = 1-5$ (parts a through e, respectively), with Xe in the threshold region as a function of kinetic energy in the center-of-mass frame (lower *x*-axis) and the laboratory frame (upper *x*-axis). A solid line shows the best fit to the data using eq 2 convoluted over the neutral and ion kinetic energy distributions. A dashed line shows the model cross sections in the absence of experimental kinetic energy broadening for reactants with an internal energy corresponding to 0 K.

The crowding of five acetonitrile molecules in the first solvent shell as found by the theoretical calculations was predicted earlier by DK.[35] They suggested that the acetonitrile molecules would show a particularly strong tendency to crowd near the ion, i.e., in the first solvent shell. Removal of an acetonitrile molecule to the second solvent shell would increase the ion-solvent molecule distance significantly because acetonitrile is a long molecule. Furthermore, because of the aprotic nature of acetonitrile, bonding of the outer shell molecule to the inner shell molecules is very weak. In attempts to examine such binding, we attempted calculations in which a fifth acetonitrile molecule was added to the second solvent shell of the $Na^+(CH_3CN)_4$ complex. During the geometry optimization calculations, the fifth acetonitrile molecule wandered around for many iterations, with almost no change in the energy of the complex until it positioned itself such that gross changes in the geometry began to occur. Through multiple attempts, these calculations always converged to the same trigonal bipyramid

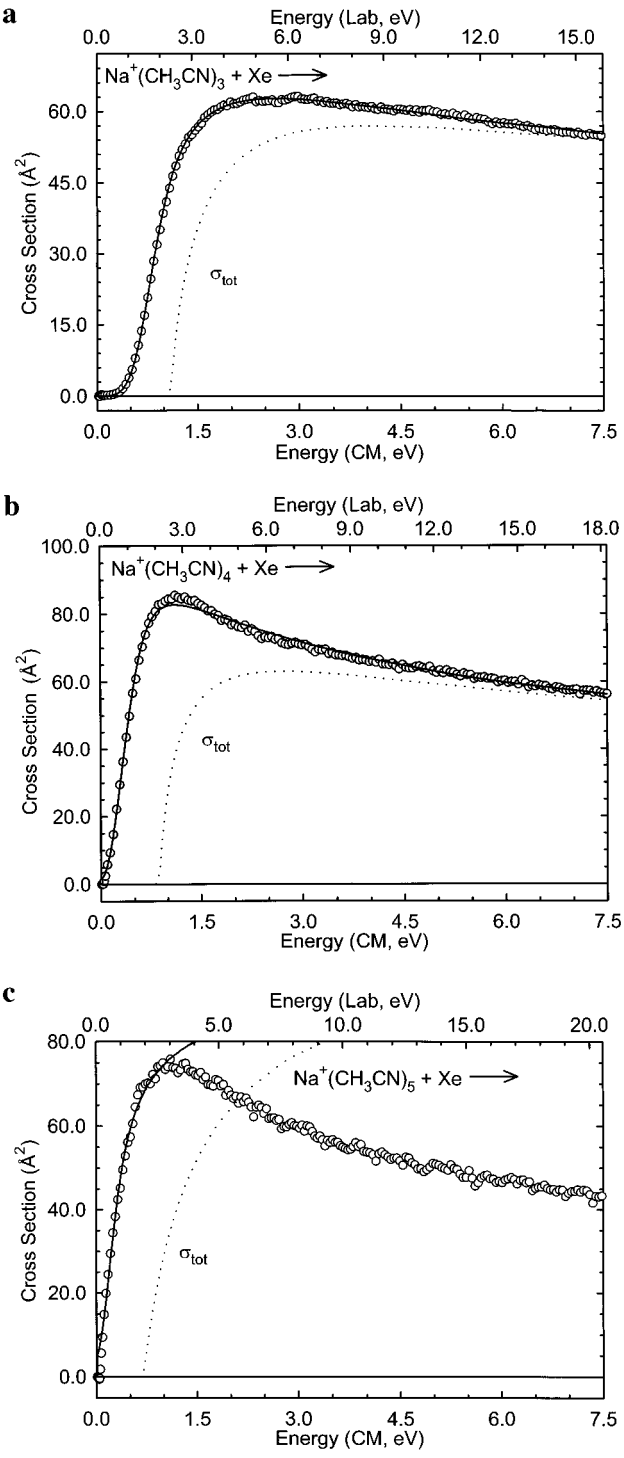

Figure 3. Zero-pressure-extrapolated total cross section for collision-induced dissociation of $Na^+(CH_3CN)_x$, $x = 3-5$ (parts a−c, respectively), with Xe in the threshold region as a function of kinetic energy in the center-of-mass frame (lower *x*-axis) and the laboratory frame (upper *x*-axis). A solid line shows the best fit to the data using eq 2 convoluted over the neutral and ion kinetic energy distributions. A dashed line shows the model cross sections in the absence of experimental kinetic energy broadening for reactants with an internal energy corresponding to 0 K.

structure shown in Figure 4 with all five acetonitrile molecules in the first solvent shell of the complex. We were unable to make $Na^+(CH_3CN)_6$ clusters experimentally; thus theoretical calculations on this complex were not pursued.

Conversion from 0 to 298 K. To allow comparison to commonly used experimental conditions, we convert the 0 K bond energies determined here (experimentally and theoretically) to 298 K bond enthalpies and free energies. The enthalpy and entropy conversions are calculated using standard formulas (assuming harmonic oscillator and rigid rotor models) and the vibrational and rotational constants determined for the MP2-(full)/6-31G* and B3LYP/6-31G* optimized geometries, which are given in Tables S1 and S2. Table 3 lists 0 and 298 K enthalpy, free energy, and enthalpic and entropic corrections for all systems experimentally determined (from Table 1). Uncertainties in the enthalpic and entropic corrections are determined by 10% variation in the molecular constants. For the $Na^+(CH_3CN)_x$ systems where the metal-ligand frequencies are very low and may not be adequately described by theory, the listed uncertainties also include scaling all frequencies below 150 cm^{-1} up and down by a factor of 2. The latter provides a conservative estimate of the computational errors in these low-frequency modes and is the dominant source of the uncertainties listed.

Discussion

Comparison of Theory and Experiment. The sequential BDEs for the $Na^+(CH_3CN)_x$, $x = 1-5$, clusters at 0 K measured here by guided ion beam mass spectrometry are summarized in Table 4. Also listed here are the 0 K BDEs calculated at both the MP2(full)/6-311+G(2d,2p)//MP2(full)/6-31G* level including full MP2 correlation, and the B3LYP/6-311+G(2d,2p)//B3LYP/6-31G* level, including zero point energy corrections and basis set superposition error corrections.[81−83] Experimental results for the $Na^+(CH_3CN)x$, $x = 1-5$, clusters taken from previous studies are also provided in Table 4 for comparison.[26,35,49] The values for $x = 3-5$ represent the values obtained from fitting the total cross section. The agreement between theory and experiment is illustrated in Figure 5.

$Na^+(CH_3CN)$. The bond energy for $Na^+(CH_3CN)$ has previously been estimated or measured by several techniques.[26,35,49] It is therefore important to carefully consider how reasonable this value is. In their work on the solvation of CH_3CN by alkali metal ions, Kebarle and co-workers[35] extrapolated a value for the $Na^+(CH_3CN)$ BDE by comparing measured values for the larger $Na^+(CH_3CN)_x$ clusters and to the $M^+(CH_3CN)_x$, $x = 1-5$, where $M^+ = K^+$, Rb^+, and Cs^+. Their extrapolated value when corrected to 0 K is within 1 kJ/mol of the value measured here, well within the experimental error of this measurement (4.5 kJ/mol). This suggests that their extrapolation technique was reasonable. In a later study, Yang and Castleman[49] deduced a binding energy for $Na^+(CH_3CN)$ in the range from 122 to 140 kJ/mol. This range spans the value measured here, including our experimental error. In a more recent study, McMahon and Ohanessian[26] performed ligand exchange equilibrium experiments in an FT-ICR to determine the binding energy of Na^+ to CH_3CN. The value they reported corrected to 0 K is 3.5 kJ/mol lower than the value determined here. This too is within experimental error of the value measured here and suggests that the value measured here is reliable. Another means of assessing the accuracy of the $Na^+(CH_3CN)$ BDE is by comparison with theory. The MP2 value lies 2.3 kJ/mol below the experimentally determined BDE, again well within the experimental error of the measured value. The value we calculated here is also consistent with the value calculated previously by McMahon and Ohanessian[26] and Hoyau et al.[34] The B3LYP value lies 8.1 kJ/mol above the experimental value, outside of the experimental error of this measurement. These results are consistent with earlier work establishing an absolute sodium ion affinity scale[34,39] in which MP2 values consistently showed better

TABLE 2: MP2(full)/6-31G* and B3LYP/6-31G* Geometry Optimized Structures of CH_3CN and $Na^+(CH_3CN)_x$, $x = 1-5$[a]

		bond length (Å)				bond angle (deg)				
species	method	Na^+−N	C≡N	C−C	C−H	NNa^+N	Na^+NC	NCC	CCH	HCH
CH_3CN	MP2	-	1.178	1.461	1.091	-	-	180.0	110.1	108.8
	B3LYP	-	1.160	1.461	1.095	-	-	180.0	110.3	108.6
$Na^+(CH_3CN)$	MP2	2.295	1.174	1.458	1.092	-	180.0	180.0	109.6	109.3
	B3LYP	2.261	1.159	1.456	1.095	-	180.0	180.0	109.8	109.1
$Na^+(CH_3CN)_2$	MP2	2.316	1.174	1.458	1.092	180.0	180.0	180.0	109.7	109.3
	B3LYP	2.290	1.158	1.457	1.095	180.0	180.0	180.0	109.9	109.1
$Na^+(CH_3CN)_3$	MP2	2.362	1.175	1.459	1.091	120.0	180.0	180.0	109.8	109.2
	B3LYP	2.340	1.158	1.458	1.094	120.0	180.0	180.0	109.9	109.0
$Na^+(CH_3CN)_4$	MP2	2.400	1.175	1.459	1.091	109.5	179.7	179.9	109.8	109.1
	B3LYP	2.387	1.158	1.459	1.094	109.5	179.8	180.0	110.0	108.9
$Na^+(CH_3CN)_5$	MP2	2.445 (3)	1.176	1.460	1.091	90.0	179.9	180.0	109.9	109.0
		2.452 (2)				120.0				
						180.0				
	B3LYP	2.443 (3)	1.158	1.460	1.094	90.0	179.9	180.0	110.1	108.8
		2.465 (2)				120.0				
						180.0				

[a] Average values are provided when there exists more than one equivalent bond length or bond angle. Deviations were small, and always less than 0.001 Å for bond lengths and 0.1° for bond angles.

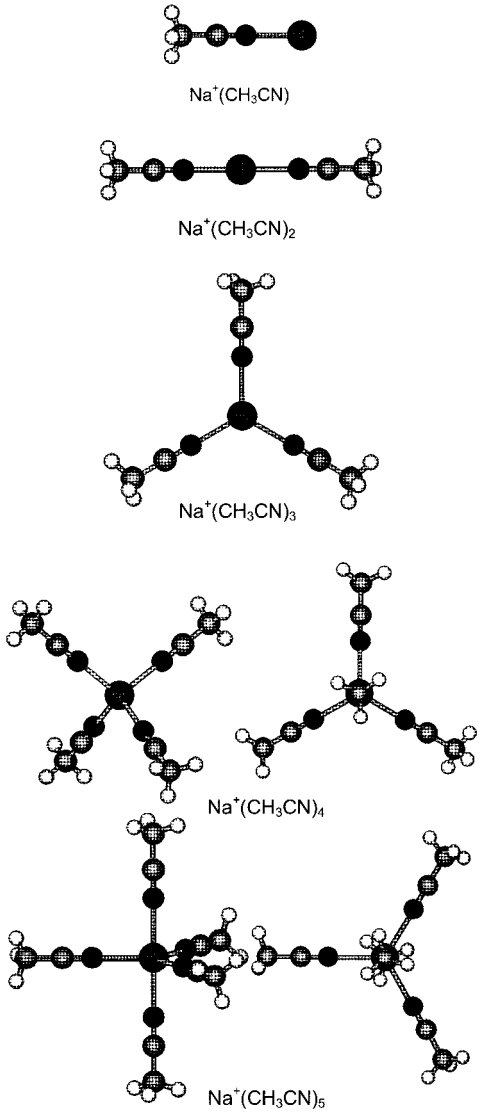

Figure 4. Optimized B3LYP/6-31G* geometries of $Na^+(CH_3CN)_x$, $x = 1-5$. Two views of the $Na^+(CH_3CN)_x$, $x = 4$ and 5, structures are shown.

agreement with experimental values (both threshold CID and high-pressure mass spectrometry) than B3LYP values. It is also consistent with the observation that the B3LYP values tend to be somewhat high for monoligated Na^+L complexes. Thus these results again suggest that where possible calculations should be performed at the MP2 level of theory or higher to obtain accurate sodium cation binding affinities.

$Na^+(CH3CN)_x$, $x = 2-5$. Our results for $Na^+(CH_3CN)_x$, $x = 2-5$, are within experimental error of the earlier values obtained by DK,[35] as can be seen in Figure 5. The average deviation between these experimental determinations is 3 ± 3 kJ/mol, well within the experimental uncertainties of these measurements. The values measured here are consistently higher than those measured by DK except for the $x = 5$ cluster where virtually identical values are measured. This suggests that all experimental measurements, ours and DK's, are reliable. The agreement between theory and experiment varies somewhat depending upon the level of theory employed and the size of the cluster. For the $Na^+(CH_3CN)_2$ cluster, the MP2 value lies 3.1 kJ/mol below the measured value, while the B3LYP value lies 3.4 kJ/mol above it. The value measured by DK lies below both theoretical values, by 4.0 and 10.5 kJ/mol for MP2 and B3LYP, respectively. This suggests that the value measured here is more reliable. For the $Na^+(CH_3CN)_3$ cluster, both theoretical values lie below the value measured here, by 10.4 and 9.6 kJ/mol for MP2 and B3LYP, respectively. Similarly, the value measure by DK is greater than both theoretical values, by 7.8 and 7.0 kJ/mol for MP2 and B3LYP, respectively. This suggests that both levels of theory underestimate the binding in this complex. For the $Na^+(CH_3CN)_4$ cluster, both theoretical values again lie below the value measured here, by 4.1 and 8.5 kJ/mol for MP2 and B3LYP, respectively. Similarly, the value measured by DK is greater than both theoretical values, by 1.8 and 6.2 kJ/mol for MP2 and B3LYP, respectively. In both cases, the differences between the experimental and theoretical values are smaller for $Na^+(CH_3CN)_4$ than that observed for the $Na^+(CH_3CN)_3$ cluster. This is somewhat difficult to understand, as it might be expected that the accuracy of theory would fall off with increasing solvation as a result of the very weak noncovalent interactions in the larger clusters requiring larger basis sets to accurately describe these weak interactions. For the $Na^+(CH_3CN)_5$ cluster, theoretical calculations could only be performed at the B3LYP level of theory. The difference between our measured value and the B3LYP value is 27.3 kJ/mol. Likewise a difference of 27.6 kJ/mol is found between DK's value and the B3LYP value. Because these differences

TABLE 3: Enthalpies and Free Energies of Binding of $Na^+(CH_3CN)_x$, $x = 1-5$ at 298 K in kJ/mol[a]

system	ΔH_0	ΔH_0	$\Delta H_{298} - \Delta H_0$	ΔH_{298}	ΔH_{298}	$T\Delta S_{298}$	ΔG_{298}	ΔG_{298}
$Na^+(CH_3CN)$	127.8 (4.5)	125.5[b]	1.1 (0.7)[b]	128.9 (4.6)	126.6[b]	26.7 (2.7)[b]	102.2 (5.3)	99.9[b]
		135.9[c]	1.1 (0.7)[c]	128.9 (4.6)	137.0[c]	26.8 (2.7)[c]	102.1 (5.3)	110.2[c]
$Na^+(CH_3CN)_2$	109.2 (7.9)	106.1[b]	−2.5 (1.4)[b]	106.7 (8.0)	103.5[b]	28.7 (8.8)[b]	78.0 (11.9)	74.8[b]
		112.6[c]	−2.5 (1.5)[c]	106.7 (8.0)	110.1[c]	30.6 (8.8)[c]	76.1 (11.9)	79.5[c]
$Na^+(CH_3CN)_3$	88.8 (2.9)	78.4[b]	−3.3 (0.6)[b]	85.8 (3.0)	75.0[b]	20.0 (8.3)[b]	65.5 (8.8)	55.0[b]
		79.2[c]	−0.6 (0.6)[c]	88.2 (3.0)	78.6[c]	30.4 (4.6)[c]	57.8 (5.5)	48.2[c]
$Na^+(CH_3CN)_4$	64.6 (2.4)	60.5[b]			58.4[b,c]			27.8[b,c]
		56.1[c]	−2.1 (0.6)[c]	62.5 (2.5)	54.0[c]	28.9 (6.4)[c]	33.6 (6.9)	25.1[c]
$Na^+(CH_3CN)_5$	52.8 (3.5)	25.5[c]	−2.4 (1.1)[c]	50.4 (3.7)	23.1[c]	36.0 (7.5)[c]	14.4 (8.3)	−12.9[c]

[a] Uncertainties are listed in parentheses. [b] Ab initio values from calculations at the MP2(full)/6-311+G(2d,2p)//MP2(full)/6-31G* level of theory with frequencies scaled by 0.9646. [c] Density functional values from calculations at the B3LYP/6-311+G(2d,2p)//B3LYP/6-31G* level of theory with frequencies scaled by 0.9804.

TABLE 4: Measured and Calculated Bond Dissociation Enthalpies of $Na^+(CH_3CN)_x$, $x = 1-5$ at 0 K in kJ/mol

	experiment		theory (MP2)			theory (B3LYP)		
complex	TCID[a]	literature	D_e[b]	D_0[c]	$D_{0,BSSE}$[d]	D_e[e]	D_0[f]	$D_{0,BSSE}$[g]
$Na^+(CH_3CN)$	127.8 (4.5)	122−140[h]	133.9	131.1	125.5	140.4	137.6	135.9
		124.3 (5.9)[i]						
$Na^+(CH_3CN)_2$	109.2 (7.9)	102.1 (4.2)[j]	117.5	114.5	106.1	118.4	115.5	112.6
$Na^+(CH_3CN)_3$	88.8 (2.9)	86.2 (4.2)[j]	87.1	85.2	78.4	83.2	81.0	79.2
$Na^+(CH_3CN)_4$	64.6 (2.4)	62.3 (4.2)[j]	69.6	67.6[f]	60.5	59.6	57.6	56.1
$Na^+(CH_3CN)_5$	52.8 (3.5)	53.1 (4.2)[j]				28.7	27.3	25.5

[a] Present results, threshold collision-induced dissociation. [b] Calculated at the MP2(full)/6-311+G(2d,2p) level of theory using MP2(full)/6-31G* optimized geometries. [c] Including zero point energy corrections with frequencies scaled by 0.9646. [d] Also includes basis set superposition error corrections. [e] Calculated at the B3LYP/6-311+G(2d,2p) level of theory using B3LYP/6-31G* optimized geometries. [f] Including zero point energy corrections with frequencies scaled by 0.9804. [g] Also includes basis set superposition error corrections. [h] Yang and Castleman.[49] [i] McMahon and Ohanessian. Adjusted to 0 K.[26] [j] Davidson and Kebarle. Adjusted to 0 K.[35]

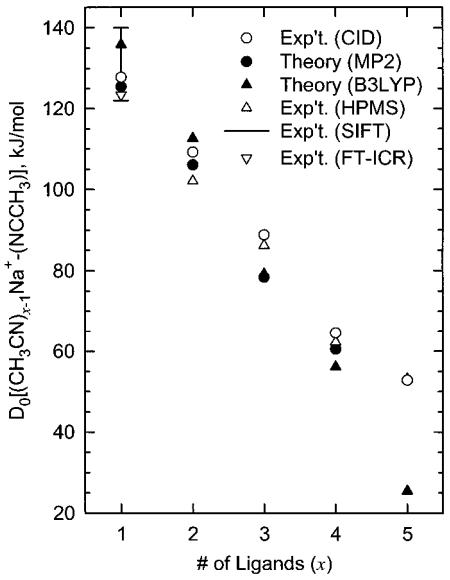

Figure 5. Experimental and theoretical bond energies at 0 K (in kJ/mol) of $[(CH_3CN)_{x-1}Na^+-NCCH_3]$ plotted versus x. Literature values for experimentally measured bond energies are taken from Davidson and Kebarle (HPMS),[35] Yang and Castleman (SIFT),[49] and McMahon and Ohanessian (FT-ICR).[26]

are much larger than observed for the smaller clusters, this suggests that an accurate description of the binding in these complexes requires higher levels of theory to describe the very weak binding of this complex.

Conclusions

The kinetic energy dependences of the collision-induced dissociation of $Na^+(CH_3CN)_x$, $x = 1-5$, with Xe are examined in a guided ion beam mass spectrometer. The dominant dissociation process in all cases is loss of an intact CH_3CN ligand. Thresholds for these processes are determined after consideration of the effects of reactant internal energy, multiple collisions with Xe, and lifetime effects (using methodology described in detail elsewhere).[40] Insight into the structures and binding energies of the $Na^+(CH_3CN)_x$ clusters is provided by ab initio and density functional theory calculations of these complexes performed at the MP2(full)/6-311+G(2d,2p)//MP2-(full)/6-31G* and B3LYP/6-311+G(2d,2p)//B3LYP/6-31G* levels of theory. The present results for the $Na^+(CH_3CN)$ cluster represents the first measurement of the bond dissociation energy for this complex. The value measured here is in excellent agreement with the extrapolated value predicted earlier by DK, the values measured by YC and MO, and the theoretical MP2 BDE. A somewhat larger deviation between the value measured for this cluster and the B3LYP theoretical value is found. These results are consistent with earlier findings for a wide variety of Na^+L complexes and suggests that this ligand can act as another reliable anchor for the sodium cation affinity scale, thus broadening the range of ligands available as absolute thermochemical anchors. Bond dissociation energies for $Na^+(CH_3CN)_x$, $x = 2-5$, agree well with previous experimental values, also suggesting that the measured thermochemistry is reliable. In addition, these system provide additional evidence that the loose PSL model used to describe the TS provides the most accurate assessment of the kinetic shifts for CID processes for electrostatic ion-molecule complexes. The agreement between theory and experiment for the larger clusters varies both with the size of the cluster and the level of theory. In general, the MP2 results appear to be more reliable than the B3LYP values. In addition, the reliability of theory tends to fall off with increasing cluster size, as it is expected that additional basis functions are required to accurately describe the very weak binding in these clusters.

Acknowledgment. This work was supported in part by an ASMS Research Award from Micromass. A.B.V. thanks the

MARC program for support under NIH Grant 5T34-GM08030-19 to Wayne State University.

Supporting Information Available: Tables of vibrational frequencies, average vibrational energies, and rotational constants for the MP2(full)/6-31G* and B3LYP/6-31G* geometry optimized structures for neutral CH_3CN and $Na^+(CH_3CN)_x$ clusters, $x = 1-5$ (PDF). This material is available free of charge via the Internet at http://pubs/acs/org.

References and Notes

(1) Glendening, E. D.; Feller, D.; Thompson, M. A. *J. Am. Chem. Soc*. **1994**, *116*, 10657.

(2) More, M. B.; Ray, D.; Armentrout, P. B. *J. Am. Chem. Soc*. **1999**, *121*, 417.

(3) Armentrout, P. B. *Int. J. Mass Spectrom*. **1999**, *193*, 227.

(4) Izatt, R. M.; Terry, R. E.; Haymore, B. L.; Hansen, L. D.; Dalley, N. K.; Avondet, A. G.; Christensen, J. J. *J. Am. Chem. Soc*. **1976**, *98*, 7620.

(5) Searles, S. K.; Kebarle, P. *Can J. Chem*. **1969**, *47*, 2619.

(6) Dzidic, I.; Kebarle, P. *J. Phys. Chem*. **1970**, *74*, 1466.

(7) Davidson, W. R.; Kebarle, P. *J. Am. Chem. Soc*. **1976**, *98*, 6133.

(8) Peterson, K. I.; Holland, P. M.; Keesee, R. G.; Lee, N.; Mark, T. D.; Castleman, A. W. *Surf. Sci*. **1981**, *106*, 136.

(9) Castleman, A. W.; Peterson, K. I.; Upschulte, B. L.; Schelling, F. J. *Int. J. Mass Spectrom. Ion Phys*. **1983**, *47*, 203.

(10) Steel, E. A.; Merz, K. M.; Selinger, A.; Castleman, A. W. *J. Phys. Chem*. **1985**, *99*, 7829.

(11) Marinelli, P. J.; Squires, R. R. *J. Am. Chem. Soc*. **1989**, *111*, 4101.

(12) Schultz, R. H.; Armentrout, P. B. *J. Phys. Chem*. **1993**, *97*, 596.

(13) Dalleska, N. F.; Honma, K.; Armentrout, P. B. *J. Am. Chem. Soc*. **1993**, *115*, 12125.

(14) Dalleska, N. F.; Tjelta, B. L.; Armentrout, P. B. *J. Phys. Chem*. **1994**, *98*, 4191.

(15) Dalleska, N. F.; Honma, K.; Sunderlin, L. S.; Armentrout, P. B. *J. Am. Chem. Soc*. **1994**, *116*, 3519.

(16) Rodgers, M. T.; Armentrout, P. B. *J. Phys. Chem. A* **1997**, *101*, 1238.

(17) Peschke, M.; Blades, A. T.; Kebarle, P. *J. Phys. Chem. A* **1998**, *102*, 2925.

(18) Peschke, M.; Blades, A. T.; Kebarle, P. *J. Phys. Chem. A* **1998**, *102*, 9978.

(19) Deng, H.; Kebarle, P. *J. Phys. Chem. A* **1998**, *102*, 571.

(20) Rodriguez-Cruz, S. E.; Jockusch, R. A.; Williams, E. R. *J. Am. Chem. Soc*. **1998**, *120*, 5842.

(21) Rodriguez-Cruz, S. E.; Jockusch, R. A.; Williams, E. R. *J. Am. Chem. Soc*. **1999**, *121*, 1986.

(22) Rodriguez-Cruz, S. E.; Jockusch, R. A.; Williams, E. R. *J. Am. Chem. Soc*. **1999**, *121*, 8898.

(23) Nielsen, S. B.; Masella, M.; Kebarle, P. *J. Phys. Chem. A* **1999**, *103*, 9891.

(24) Peschke, M.; Blades, A. T.; Kebarle, P. *J. Am. Chem. Soc*. **2000**, *122*, 10440.

(25) Anvia, F.; Walsh, S.; Capon, M.; Koppel, I. A.; Taft, R. W.; de Paz, J. L. G.; Catalan, J. *J. Am. Chem. Soc*. **1990**, *112*, 5095. Taft, R. W.; Anvia, F.; Gal, J.-F.; Walsh, S.; Capon, M.; Holmes, M. C.; Hosn, K.; Oloumi, G.; Vasanwala, R.; Yazdani, S. *Pure Appl. Chem*. **1990**, *62*, 17. Burk, P.; Koppel, I. A.; Koppel, I.; Kurg, R.; Gal, J.-F.; Maria, P.-C.; Herreros, M.; Notario, R.; Abboud, J.-L. M.; Anvia, F.; Taft, R. W. *J. Phys. Chem. A* **2000**, *104*, 2824.

(26) McMahon, T. B.; Ohanessian, O. *Chem. Eur. J*. **2000**, *6*, 2931.

(27) Guo, B. C.; Conklin, B. J.; Castleman, A. W. *J. Am. Chem. Soc*. **1989**, *111*, 6506.

(28) Leuchtner, R. E.; Farley, R. W.; Harms, A. C.; Funasaka, H.; Castleman, A. W. *Int. J. Mass Spectrom. Ion Processes* **1990**, *102*, 199.

(29) Guo, B. C.; Castleman, A. W. *Int. J. Mass Spectrom. Ion Processes* **1990**, *100*, 665.

(30) Andersen, A.; Muntean, F.; Walter, D.; Rue, C.; Armentrout, P. B. *J. Phys. Chem. A* **2000**, *104*, 692.

(31) Rodgers, M. T.; Armentrout, P. B. *J. Phys. Chem. A* **1997**, *101*, 2614.

(32) Rodgers, M. T.; Armentrout, P. B. *J. Phys. Chem. A* **1999**, *103*, 4955.

(33) Rodgers, M. T.; Armentrout, P. B. *J. Chem. Phys*. **1998**, *109*, 1787.

(34) Hoyau, S.; Norrman, K.; McMahon, T. B.; Ohanessian, G. *J. Am. Chem. Soc*. **1999**, *121*, 8864.

(35) Davidson, W. R.; Kebarle, P. *J. Am. Chem. Soc*. **1976**, *98*, 6125.

(36) Deng, H.; Kebarle, P. *J. Am. Chem. Soc*. **1998**, *120*, 2925.

(37) Shoeib, T.; Houssain, E. A.; Siu, K. W. M.; Hopkinson, A. C. *J. Phys. Chem A* **2001**, *105*, 710.

(38) Jarek, R. L.; Miles, T. D.; Trester, M. L.; Denson, S. C.; Shin, S. K. *J. Phys. Chem. A* **2000**, *104*, 2230.

(39) Armentrout, P. B.; Rodgers, M. T. *J. Phys. Chem. A* **2000**, *104*, 2238.

(40) Rodgers, M. T.; Ervin, K. M.; Armentrout, P. B. *J. Chem. Phys*. **1997**, *106*, 4499.

(41) Rodgers, M. T.; Armentrout, P. B. *Int. J. Mass Spectrom*. **1999**, *185/186/187*, 359.

(42) Amunugama, R.; Rodgers, M. T. *Int. J. Mass Spectrom*. **2000**, *195/196*, 439.

(43) Rodgers, M. T.; Armentrout, P. B. *J. Am. Chem. Soc*. **2000**, *122*, 8548.

(44) Rodgers, M. T.; Stanley, J. R.; Amunugama, R. *J. Am. Chem. Soc.* **2000**, *122*, 10969.

(45) Rodgers, M. T. *J. Phys. Chem. A* **2001**, *105*, 2374.

(46) Amunugama, R.; Rodgers, M. T. *J. Phys. Chem. A* **2001**, *105*, 9883.

(47) Rodgers, M. T. *J. Phys. Chem. A* **2001**, *105*, 8145.

(48) Rodgers, M. T.; Armentrout, P. B. *J. Am. Chem. Soc.*, submitted for publication.

(49) Yang, X.; Castleman, A. W. *J. Chem. Phys*. **1990**, *93*, 2405.

(50) Teloy, E.; Gerlich, D. *Chem. Phys.* **1974**, *4*, 417. D. Gerlich, Diplomarbeit, University of Freiburg, Federal Republic of Germany, 1971. Gerlich, D. In *State-Selected and State-to-State Ion−Molecule Reaction Dynamics, Part I, Experiment*; Ng, C.-Y., Baer, M., Eds.; *Adv. Chem. Phys.* **1992**, *82*, 1.

(51) Dalleska, N. F.; Honma, K.; Armentrout, P. B. *J. Am. Chem. Soc.* **1993**, *115*, 12125.

(52) Aristov, N.; Armentrout, P. B. *J. Phys. Chem*. **1986**, *90*, 5135.

(53) Hales, D. A.; Armentrout, P. B. *J. Cluster Sci*. **1990**, *1*, 127.

(54) Ervin, K. M.; Armentrout, P. B. *J. Chem. Phys.* **1985**, *83*, 166.

(55) Dalleska, N. F.; Honma, K.; Sunderlin, L. S.; Armentrout, P. B. *J. Am. Chem. Soc*. **1994**, *116*, 3519.

(56) Schultz, R. H.; Armentrout, P. B. *J. Chem. Phys*. **1992**, *96*, 1046.

(57) Schultz, R. H.; Crellin, K. C.; Armentrout, P. B. *J. Am. Chem. Soc.* **1992**, *113*, 8590.

(58) Khan, F. A.; Clemmer, D. C.; Schultz, R. H.; Armentrout, P. B. *J. Phys. Chem*. **1993**, *97*, 7978.

(59) Fisher, E. R.; Kickel, B. L.; Armentrout, P. B. *J. Phys. Chem*. **1993**, *97*, 10204.

(60) Beyer, T. S.; Swinehart, D. F. *Comm. Assoc. Comput. Machines* **1973**, *16*, 379. Stein, S. E.; Rabinovitch, B. S. *J. Chem. Phys*. **1973**, *58*, 2438; *Chem. Phys. Lett*. **1977**, *49*, 1883.

(61) Pople, J. A.; Schlegel, H. B.; Raghavachari, K.; DeFrees, D. J.; Binkley, J. F.; Frisch, M. J.; Whitesides, R. F.; Hout, R. F.; Hehre, W. J. *Int. J. Quantum Chem. Symp*. **1981**, *15* 269. DeFrees, D. J.; McLean, A. D. *J. Chem. Phys*. **1985**, *82*, 333.

(62) Waage, E. V.; Rabinovitch, B. S. *Chem. Rev*. **1970**, *70*, 377.

(63) Chesnavich, W. J.; Bowers, M. T. *J. Phys. Chem.* **1979**, *83*, 900.

(64) Armentrout, P. B. In *Advances in Gas-Phase Ion Chemistry*; Adams, N. G., Babcock, L. M., Eds.; JAI: Greenwich, 1992; Vol. 1, pp 83−119.

(65) See, for example: Sunderlin, L. S.; Armentrout, P. B. *Int. J. Mass Spectrom. Ion Processes* **1989**, *94*, 149.

(66) More, M. B.; Glendening, E. D.; Ray, D.; Feller, D.; Armentrout, P. B. *J. Phys. Chem.* **1996**, *100*, 1605.

(67) Ray, D.; Feller, D.; More, M. B.; Glendening, E. D.; Armentrout, P. B. *J. Phys. Chem.* **1996**, *100*, 16116.

(68) Meyer, F.; Khan, F. A.; Armentrout, P. B. *J. Am. Chem. Soc*. **1995**, *117*, 9740.

(69) See, for example: Figure 1 in Dalleska, N. F.; Honma, K.; Armentrout, P. B. *J. Am. Chem. Soc*. **1993**, *115*, 12126.

(70) Armentrout, P. B.; Simons, J. *J. Am. Chem. Soc*. **1992**, *114*, 8627.

(71) Frisch, M. J.; Trucks, G. W.; Schlegel, H. B.; Scuseria, G. E.; Robb, M. A.; Cheeseman, J. R.; Zakrzewski, V. G.; Montgomery, J. A., Jr.; Stratmann, R. E.; Burant, J. C.; Dapprich, S.; Millam, J. M.; Daniels, A. D.; Kudin, K. N.; Strain, M. C.; Farkas, O.; Tomasi, J.; Barone, V.; Cossi, M.; Cammi, R.; Mennucci, B.; Pomelli, C.; Adamo, C.; Clifford, S.; Ochterski, J.; Petersson, G. A.; Ayala, P. Y.; Cui, Q.; Morokuma, K.; Malick, D. K.; Rabuck, A. D.; Raghavachari, K.; Foresman, J. B.; Cioslowski, J.; Ortiz, J. V.; Stefanov, B. B.; Liu, G.; Liashenko, A.; Piskorz, P.; Komaromi, I.; Gomperts, R.; Martin, R. L.; Fox, D. J.; Keith, T.; Al-Laham, M. A.; Peng, C. Y.; Nanayakkara, A.; Gonzalez, C.; Challacombe, M.; Gill, P. M. W.; Johnson, B. G.; Chen, W.; Wong, M. W.; Andres, J. L.; Head-Gordon, M.; Replogle, E. S.; Pople, J. A. *Gaussian 98*, revision A.7; Gaussian, Inc.: Pittsburgh, PA, 1998.

(72) Because of limitations of our computational resources, we were unable to perform a vibrational analysis at the MP2(full)/6-31G* level for the $Na^+(CH_3CN)_4$ cluster, were not able to perform MP2(full)/6-31G* calculations for the $Na^+(CH_3CN)_5$ cluster, and were forced to resort to density functional calculations for these systems. Thus density functional calculations were performed for all clusters for consistency.

(73) Becke, A. D. *J. Chem. Phys.* **1993**, *98*, 5648.

(74) Lee, C.; Yang, W.; Parr, R. G. *Phys. Rev. B* **1988**, *37*, 785.

(75) Foresman, J. B.; Frisch, Æ. *Exploring Chemistry with Electronic Structure Methods*, 2nd ed.; Gaussian: Pittsburgh, PA, 1996.
(76) Boys, S. F.; Bernardi, R. *Mol. Phys.* **1979**, *19*, 553.
(77) Van Duijneveldt, F. B.; van Duijneveldt-van de Rijdt, J. G. C. M.; van Lenthe, J. H. *Chem. Rev.* **1994**, *94*, 1873.
(78) Feller, D.; Glendening, E. D.; Kendall, R. A.; Peterson, K. A. *J. Chem. Phys*. **1994**, *100*, 49881.
(79) Lifshitz, C. *Adv. Mass Spectrom*. **1989**, *11*, 113.
(80) Figures were generated using the output of Gaussian98 geometry optimizations in Hyperchem Computational Chemistry Software Package, Version 5.0, Hypercube Inc., 1997.
(81) Møller, C.; Plesset, M. S. *Phys. Rev*. **1934**, *46*, 618.
(82) Bartlett, R. J. *Annu. Rev. Phys. Chem.* **1981**, *32*, 359.
(83) Hehre, W. J.; Radom, L.; Schleyer, P. v. R.; Pople, J. A. *Ab Initio Molecular Orbital Theory*; Wiley: New York, 1986.